

See discussions, stats, and author profiles for this publication at: <https://www.researchgate.net/publication/275956355>

Low stiffness tactile transducers based on AlN thin film and polyimide

ARTICLE *in* APPLIED PHYSICS LETTERS · APRIL 2015

Impact Factor: 3.3

READS

30

7 AUTHORS, INCLUDING:



Vincenzo Mariano Mastronardi

Istituto Italiano di Tecnologia

5 PUBLICATIONS 3 CITATIONS

SEE PROFILE



Luca Ceseracciu

Istituto Italiano di Tecnologia

46 PUBLICATIONS 386 CITATIONS

SEE PROFILE



Francesco Rizzi

Istituto Italiano di Tecnologia

34 PUBLICATIONS 155 CITATIONS

SEE PROFILE



Simona Petroni

Istituto Italiano di Tecnologia

21 PUBLICATIONS 90 CITATIONS

SEE PROFILE

Low stiffness tactile transducers based on AlN thin film and polyimide

V. M. Mastronardi, L. Ceseracciu, F. Guido, F. Rizzi, A. Athanassiou, M. De Vittorio, and S. Petroni

Citation: [Applied Physics Letters](#) **106**, 162901 (2015); doi: 10.1063/1.4918749

View online: <http://dx.doi.org/10.1063/1.4918749>

View Table of Contents: <http://scitation.aip.org/content/aip/journal/apl/106/16?ver=pdfcov>

Published by the [AIP Publishing](#)

Articles you may be interested in

[Deposition of highly textured AlN thin films by reactive high power impulse magnetron sputtering](#)

J. Vac. Sci. Technol. A **33**, 021518 (2015); 10.1116/1.4907874

[Ultrafast optical technique for measuring the electrical dependence of the elasticity of piezoelectric thin film: Demonstration on AlN](#)

Rev. Sci. Instrum. **84**, 015007 (2013); 10.1063/1.4788936

[Epitaxial growth and orientation of AlN thin films on Si\(001\) substrates deposited by reactive magnetron sputtering](#)

J. Appl. Phys. **100**, 123514 (2006); 10.1063/1.2402971

[Characterization of nanotextured AlN thin films by x-ray absorption near-edge structures](#)

Appl. Phys. Lett. **86**, 163113 (2005); 10.1063/1.1904714

[Effect of intrinsic stress on preferred orientation in AlN thin films](#)

J. Appl. Phys. **95**, 2130 (2004); 10.1063/1.1640462

The advertisement features a dark blue background with three images: a mobile phone, a desktop computer, and an AFM. Text on the left asks why one would still use these older technologies. Text on the right promotes upgrading to a modern AFM with a trade-in discount and identifies Asylum Research as the leader in AFM technology. The Oxford Instruments logo and contact information are at the bottom right.

You don't still use this cell phone

or this computer

Why are you still using an AFM designed in the 80's?

It is time to upgrade your AFM

Minimum \$20,000 trade-in discount for purchases before August 31st

Asylum Research is today's technology leader in AFM

dropmyoldAFM@oxinst.com

OXFORD INSTRUMENTS
The Business of Science®

Low stiffness tactile transducers based on AlN thin film and polyimide

V. M. Mastronardi,^{1,2,a)} L. Ceseracciu,³ F. Guido,^{1,4} F. Rizzi,¹ A. Athanassiou,³
 M. De Vittorio,^{1,4} and S. Petroni¹

¹Center for Biomolecular Nanotechnologies at UNILE, Istituto Italiano di Tecnologia, Via Barsanti,
 73010 Arnesano, LE, Italy

²Dip. Scienza Applicata e Tecnologia, Politecnico di Torino, Torino 10129, Italy

³Smart Materials, Istituto Italiano di Tecnologia, via Morego, 16163 Genova, Italy

⁴Dip. Ingegneria dell'Innovazione, Università del Salento, Lecce 73100, Italy

(Received 18 March 2015; accepted 10 April 2015; published online 20 April 2015)

In this paper, we propose a flexible piezoelectric MEMS transducer based on aluminum nitride thin film grown on polyimide soft substrate and developed for tactile sensing purposes. The proposed device consists of circular micro-cells, with a radius of 350 μm , made of polycrystalline c-axis textured AlN. The release of compressive stress by crystalline layers over polymer substrate allows an enhanced transduction response when the cell is patterned in circular dome-shaped geometries. The fabricated cells show an electromechanical response within the full scale range of 80 mN (≈ 200 kPa) both for dynamic and static load. The device is able to detect dynamic forces by exploiting both piezoelectric and flexoelectric capabilities of the aluminum nitride cells in a combined and synergistic sensing that occurs as voltage generation. No additional power supply is required to provide the electrical readout signals, making this technology suitable candidate when low power consumption is demanding. Moreover a capacitance variation under constant stress is observed, allowing the detection of static forces. The sensing ability of the AlN-based cells has been tested using an *ad hoc* setup, measuring both the applied load and the generated voltage and capacitance variation. © 2015 AIP Publishing LLC. [<http://dx.doi.org/10.1063/1.4918749>]

Artificial tactile systems for pressure and force measurements are important in many applications as automated assembling, machining, sorting, and stacking production; in minimal invasive medical procedures (MIS) for the evaluation of tissues stiffness and damages; in prosthetic and orthotic devices where artificial skin restores loss of tactile sensations. Similarly, humanoid robots need tactile interface devices for a safe interaction with humans in assisting activities. Equipping a robot with specific sensors and transducers is a way to confer him sufficient autonomy to perform tasks in unstructured environments. Unlike other senses, tactile sensory system provides information on physical properties of different nature such as shape, texture, and stiffness (to control the manipulation with optimal forces), which is not easily achieved by vision alone. Also during grasping and manipulation of objects, the right tactile perception prevents slippage and damage (ensuring the manual dexterity in a robotic system). An artificial tactile system that emulates these abilities and performs advanced in-hand manipulation tasks should detect dynamic forces, such as normal and tangential contact for gathering spatial and geometrical information from surfaces exploration, as well as static forces. To this aim, arrays of pressure-sensitive sensors should be integrated on the robot fingertips as an electronic skin and flexibility and stretchability are desirable properties to increase the anthropomorphism.

In the last decades, several technological approaches have been used to realize a low-cost, large-area-compatible artificial skin, suitable for object manipulation, and with sufficient sensitivity in a wide pressure range (10–100 kPa).

One promising approach is based on MEMS exploiting the high sensitivity to inertial forces and a consolidated electronics of readout. In general, tactile MEMS are based on silicon and they detect inertial forces by capacitance variation or resistance variation^{1,2} of strain gauges. MEMS sensors show high spatial resolution, reliable response and linearity, but they are brittle and not suitable for large deformations and coverage of curved three-dimensional surfaces. To overcome this limit, tactile sensors have been integrated on various polymer-based materials as flexible substrates to make them able to bend, expand, and adapt on irregular surfaces.³

These polymer-based sensors exploit several sensing mechanisms like resistive,³ capacitive,^{4–6} and piezoresistive.^{7–9} They are usually fabricated using standard MEMS technologies such as thin film deposition, plasma etching, and photolithography. These sensors have good resolution, reliable response, and high accuracy,^{10–12} but often due to the viscoelasticity of the polymers they suffer from hysteresis and crosstalk. Among them, piezoelectric sensors appear to be very attractive because of their low power consumption and in same case low thermal budgets for materials deposition as for Aluminum Nitride (AlN) and Zinc Oxide (ZnO). In particular, AlN is a promising piezoelectric material for flexible technology,^{13–17} since it does not need to be electrically poled, differently from the widely used ferroelectric materials like Lead Zirconium Titanate (PZT) or polyvinylidene fluoride (PVDF). The c-axis oriented polycrystalline columnar structure of AlN exhibits moderate piezoelectric coefficient, high thermal conductivity (200 W/mK), low dielectric constant (≈ 9), high electrical resistivity, and high temperature stability (up to 1500 °C).^{18,19}

In this study, we present AlN tactile transducers realized on Kapton[®] by standard micromachining process, where the

^{a)}Electronic mail: vincenzo.mastronardi@iit.it

stress release of the active layers (Mo, AlN) generates an uplifted dome with a structural stiffness well below the stiffness of composing materials. The electrical and mechanical characterization with *ad hoc* setup shows they are sensitive to periodic impulsive mechanical stimuli by virtue of a synergistic interaction between flexoelectric and piezoelectric effects.^{20–22} The dielectric properties of the Mo/AlN/Mo stack, which behaves as a capacitor, allows to measure long static mechanical stimuli by a steady deformation of the convex structure.

The process flow of AlN transducers fabrication is shown in Fig. 1(a). The Mo(150 nm)/AlN(\approx 900 nm) structure has been deposited by sputtering on 25 μ m thick polyimide substrate, then the AlN film has been patterned in circular shape with a diameter of 700 μ m. The Mo bottom electrode has been patterned by wet etching with hydrogen peroxide solution (30%). Subsequently, molybdenum top electrodes (250 nm) have been structured by lift-off technique (details on microfabrication are reported elsewhere^{13,14,23}). A parylene C coating of 1 μ m has been deposited via CVD deposition as protective layer to prevent external damages and to electrically isolate the transducers. The map of Fig. 1(b) shows that the release of the compressive residual stress of the thin layers generates a dome structure on the polymer after dry etching.²³ The domes are lifted up with an average height of $h_m = 38 \pm 5 \mu$ m over the substrate base (blue region in Fig. 1(b)). The estimated average radius of the uplifted region is $r_{up} = 1.37 \pm 0.16$ mm, whereas the radius of AlN cells is $r = 350 \mu$ m.

In the parylene C coating, vias have been opened and the electrodes have been bonded to a printed circuit board (PCB) testing platform. Fig. 1(c) shows the prototype, ready for electromechanical testing.

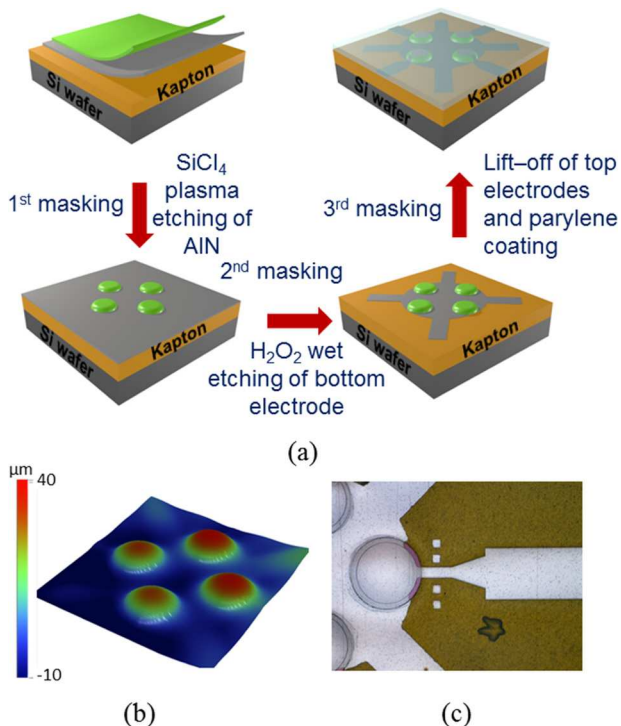


FIG. 1. (a) Fabrication process of the force transducers. (b) 3D profile mapping. (c) Optical image of a single dome.

The sensing mechanism mainly relies on the dome shape; when a normal force is applied on the top of the dome, a mechanical stress occurs in the AlN thin layer that becomes electrically polarized due to both piezoelectric and flexoelectric effects. The total electric polarization P_i induced by the two effects is described by the following equation:

$$P_i = d_{ijk}\sigma_{jk} + \mu_{ijkl} \frac{\partial \varepsilon_{jk}}{\partial x_l}, \quad (1)$$

where d_{ijk} is the appropriate piezoelectric coefficient along the axis of the applied stress σ_{jk} in the relevant direction specified by k and j indexes, μ_{ijkl} is the flexoelectric constant, ε_{jk} is the strain, and x_l is the position coordinate.

The study on the impulsive dynamic stress detection has been performed by using the XYZTEC Condor EZ push and pull system (the schematic is shown in Fig. 2) and connecting the transducer terminals to an oscilloscope (Tektronix MDO4000). Load has been applied with a stainless steel cylindrical straight rod, whose diameter was 1 mm. Before testing, the frame stiffness has been measured as 55.6 N/mm, much higher than the devices. For this reason, it can be assumed that the reported deformation occurs in the dome-shaped structures and not in the set-up. The pushing probe was equipped with a load cell, able to detect reaction forces from 0.49 mN to 490 mN.

Two representative dome-shaped devices, characterized by different releasing height as displayed in the 2D profile of Fig. 3(a), have been electrically characterized. The 2D profilometry points out that the compressive stress is released in a perfectly curved dome and an up-lifted annular region. These measurements suggest a different detachment of the dome from the silicon substrate and, as a consequence, a different empty space for both domes between polyimide and silicon substrate, a larger annular region for the higher dome and a smaller annular region for the lower dome (see measured geometrical parameters in Table I). Hereafter, larger dome is called Dome-A and smaller dome is called Dome-B (Fig. 3(a)). It will be shown below the relationship between the electromechanical response and the individual stiffness of each dome due to the different shape. In Fig. 3(b), the

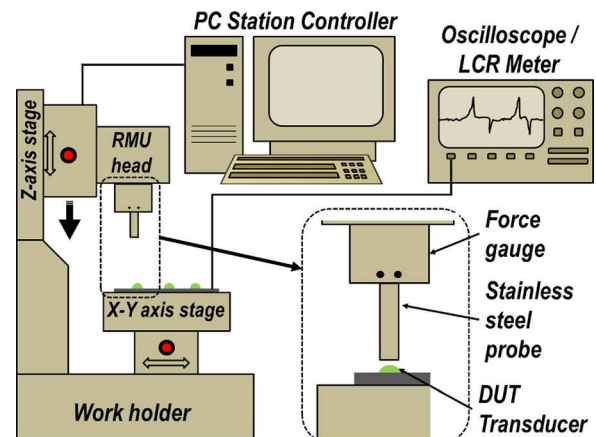


FIG. 2. Schematic of the apparatus to evaluate the output response of the transducers. The peak voltage is measured with an oscilloscope, whereas the capacitance variation is measured with a precision LCR-meter.

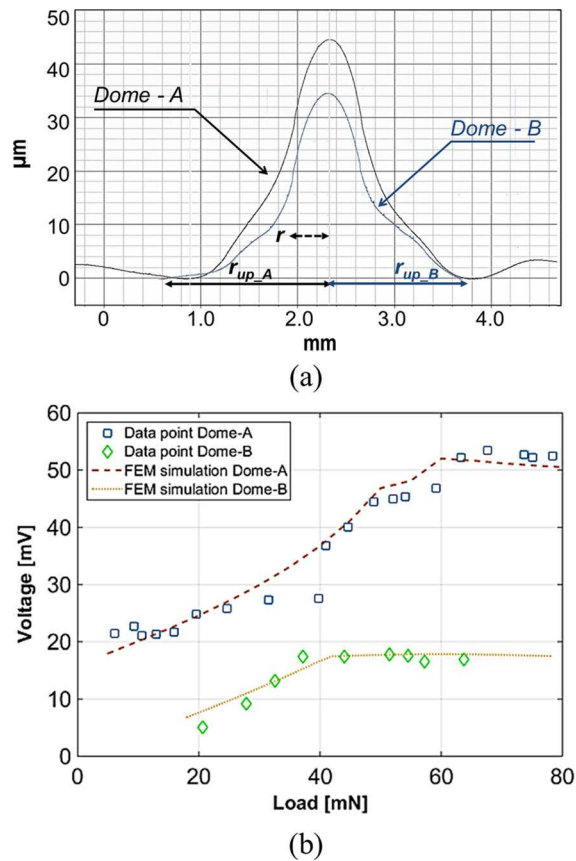


FIG. 3. (a) 2D profile of Dome-A and Dome-B; r_{up} , r , and dome height are listed in Table I. (b) Measured voltage output for Dome-A and Dome-B. Data points refer to measured values and dot lines are the FEM simulation results.

electrical characterization results are plotted; the output voltage at the peak is reported vs the applied force, both for Dome-A and Dome-B.

Each data point is the average of three measurements with the same force and penetration depth, collected at a frequency of 0.3 Hz (with approach velocity of the pushing probe of $600 \mu\text{m/s}$ and hold time of 200 ms). The electromechanical behavior of domes is similar and it is due to the combination of both piezoelectric and flexoelectric effects. For Dome-A, an offset of 18 mV in the measured voltage has been observed. The Dome-A shows an increase of generated voltage in a dynamic range of [0–60 mN], while Dome-B dynamic range is characterized by a linear increase up to 40 mN, starting from the minimum detected force of 20 mN; a lower offset has been observed. For higher applied forces, both devices start to saturate when the force reaches the threshold value of ≈ 60 mN for Dome-A and ≈ 40 mN for Dome-B, respectively. The voltage range generated from Dome-A shows a maximum value of ≈ 50 mV and from Dome-B ≈ 25 mV; a sensitivity of approximately 480 mV/N

and 445 mV/N in the linear dynamic range before saturation is observed, respectively. The minimum force detected is ≈ 1.2 mN.

The detection of long static stimuli has been experimentally observed as capacitance decrease ΔC at increasing forces that have been applied by using the setup showed in Fig. 2. ΔC has been then collected by a precision LCR-meter (Agilent E4980A). The results are reported in Fig. 4 as the modulus of ΔC , with an initial measured capacitance of 43.9 pF for Dome-A and 41.6 pF for Dome-B, when no load is applied. For each point, the displacement of the z-axis stage has been slowly increased with a step resolution of $1 \mu\text{m}$ up to a total depth of $25 \mu\text{m}$. Each data point is the average of three measurements with the same force and penetration depth. The approach velocity of the probe, held on the sensing element for 1 s, is $10 \mu\text{m/s}$. The capacitance variation has been observed for the whole interval of application of the stress and it does not decay with time; therefore, static forces detection is possible in the same system, making the AlN thin film in dome structure a multifunctional material. Fig. 4 shows a significant response to long static stimuli in the force range up to 80 mN, in which the achieved sensitivity in static sensing mode has been evaluated as 950 fF/N for Dome-A and 620 fF/N for Dome-B.

The shape and the mechanical stiffness of the structure are the reference parameters useful for explaining the electromechanical response of the transducers. The dome structural stiffness, considered as resistance to bending of the tetra-layered domes, has been measured through the XYZTEC push tester. In this test, the z-axis stage has been moved down with a velocity of $10 \mu\text{m/s}$. Stiffness k_s as a structure property has been, therefore, assessed as the slope of the load-deformation curve and it has been extracted as the slope of the linearly fitted load-depth curve of loading, up to 80 mN. In this deformation region, results show a stiffness of $k_{sA} \approx 3.5$ N/mm for Domes-A and $k_{sB} \approx 9.7$ N/mm for Domes-B. Despite extreme flexibility, the Mo/AlN/Mo multilayered structure results to be robust even after several cycles of bending by virtue of peculiar mechanical properties derived from the combination of materials with different elasticity. Table I summarizes the geometrical parameters, the measured stiffness and the normal stress sensitivity. The low value of k_s , compared to the stiffness of bulk materials included in the structure, is not only due to the fabricated tetra-layered structure but also due to the part of the surrounding polymer that is uplifted by the differential shrinkage. The structure compliance can, therefore, be split in the sum of two contributions with the central area treated as a fixed membrane and the outer area as an annular membrane, fixed in the outer edge and guided in the inner edge. The overall displacement can be expressed considering the compliance as the series of both contributions²⁴

TABLE I. Measured geometrical parameters r , r_{up} , and h , measured stiffness k_s , and dynamic (SI_d) and static (SI_s) normal stress sensitivity.

Dome	Radius r (μm)	Uplifted radius r_{up} (mm)	Height h (μm)	Stiffness k_s (N/mm)	Dynamic stress sensitivity SI_d (mV/N)	Static stress sensitivity SI_s (fF/N)
Dome-A	350	1.53	43	3.50	480	950
Dome-B	350	1.21	33	9.70	445	620

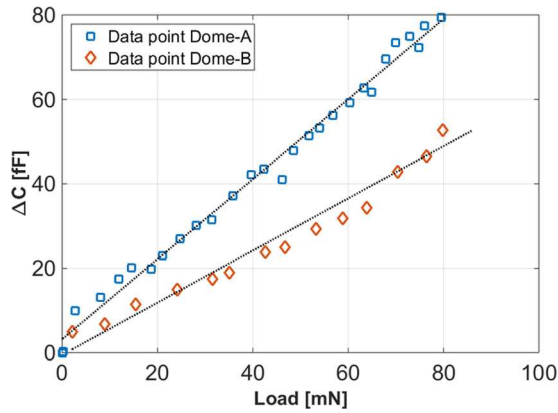


FIG. 4. Relationship between applied force and capacitance decrease ΔC for the long static stimuli detection.

$$y = F \left(\frac{r^2}{16\pi k_i} + c \frac{r_{up}^2}{k_{up}} \right), \quad (2)$$

where k is the bending stiffness, according to the simple membrane model

$$k = \frac{Et^3}{12(1 - \nu^2)}, \quad (3)$$

with the subscripts i for the inner part and up for the uplifted region; F is the applied load, c is a correction parameter adjusted to the ratio r_{up}/r , E is the Young's modulus, and ν is the Poisson ratio. Despite the simplicity of the model, the values of modeled stiffness, namely, $k_{sAmodel} = 3.1 \text{ N/mm}$ and $k_{sBmodel} = 8.2 \text{ N/mm}$, are in reasonable agreement with the measurements of both A and B systems ($\Delta k_A \simeq 13\%$ and $\Delta k_B \simeq 18\%$), as summarized in Table I. The effect of the uplifted area size is clear from Eq. (2): the larger the radius of the outer area, the lower the stiffness of the dome as a whole allowing an electromechanical response of the piezo-cells Dome-A at low forces (6–20mN), as shown in Fig. 3(a). In the same range, due to the higher stiffness of Dome-B, no electromechanical response (both piezo and flexo polarization) is measured while load is applied. Analogously, the stiffer Dome-B shows a lower capacitance variation with respect to Dome-A (Fig. 4).

Finite element method (FEM) simulations have been implemented in order to understand the different electromechanical behavior and dynamic range shown in Fig. 3(b) between the domes. The implemented multiphysics was the combination of structural mechanics and piezoelectricity, while the flexoelectricity has been kept in account as the measured offset. The exploited physics for the simulations of the structure has been the structural mechanics and the electrostatics to simulate the piezoelectric multi-physics and to estimate the electromechanical response of the device. The geometry has been built by a 2D axial symmetry, in which the axis corresponds to the center of the dome. A standard free triangular mesh has been set up as finite element geometry discretization and a stationary study has been performed to solve the electromechanical analysis for each applied load. The normalized calculated voltage has been superimposed to the measured signal for comparison. For the higher

Dome-A and load in the range up to 60 mN, simulations show the dome is pushed downwards, with slight compression in polyimide substrate tape, until the released structure is flattened on the silicon substrate. In this region, the stress is transferred to the piezoelectric film, generating the voltage signal. For forces higher than 60 mN, the constant flattening causes the signal saturation. For the lower Dome-B, simulations confirm the same mechanism. Its flattening region has been identified in the range up to 40 mN. Once flattened, Dome-B behaves as Dome-A, showing saturation.

In summary, we proposed and developed dome shaped piezoelectric transducers realized by integration of high Young modulus material as Aluminum Nitride on a low modulus material as polyimide. The integration results in a natural three-dimensional bowed structure due to the compressive residual stress of AlN on the polymeric substrate. The stress release provides a perfectly curved dome and an uplifted area of polyimide substrate. As confirmed by the analytical model and by FEM simulations, the uplifted area is determinant for low stiffness and dynamic range of the transducer that easily deforms under loading. Further investigation of the robustness of the multilayered structure is needed to prove the cyclic electromechanical response of the transducers. Preliminary measurements demonstrate that the transducer detects dynamic contact forces, by exploiting the combination of both piezoelectric and flexoelectric effect in the same material, in the range up to 60 mN before saturation and static contact forces (up to 1 s of applied mechanical load) by capacitance decrease in a range up to 80 mN. Furthermore, the estimated sensitivity to normal stress in dynamic sensing mode is up to 480 mN/V and in static sensing mode is up to 950 fF/N. The results are encouraging and the technology is well suited to realize large area tactile sensors for robotics applications.

This research is funded by ITEM Program Infrastructure for BioMEMS technologies of advanced sensing for environmental and food monitoring and diagnostic (PONa3_00077).

- ¹B. J. Kane, M. R. Cutkosky, and G. T. A. Kovacs, *IEEE J. Microelectromech. Syst.* **9**(4), 425 (2000).
- ²C. L. Dai, P. W. Lu, C. Chang, and C. Y. Liu, *Sensors* **9**(12), 10158 (2009).
- ³E. S. Hwang, J. H. Seo, and Y. J. Kim, *J. Microelectromech. Syst.* **16**, 556 (2007).
- ⁴H. K. Lee, J. Chung, S. I. Chang, and E. Yoon, *J. Microelectromech. Syst.* **17**, 934 (2008).
- ⁵M. Y. Chang, C. L. Lin, Y.-T. Lai, and Y. J. Yang, *Sensors* **10**(11), 10211 (2010).
- ⁶M. Y. Cheng, X. H. Huang, C. W. Ma, and Y. J. Yang, *J. Micromech. Microeng.* **19**(11), 115001 (2009).
- ⁷J. Castellanos-Ramos, R. Navas-Gonzalez, H. Macicior, T. Sikora, E. Ochoteco, and F. Vdal-Verdu, *Microsyst. Technol.* **16**(5), 765 (2010).
- ⁸K. Noda, K. Hoshino, K. Matsumoto, and I. Shimoyama, *Sens. Actuators, A* **127**(2), 295 (2006).
- ⁹H. Takahashi, A. Nakai, N. Thanh-Vinh, K. Matsumoto, and I. Shimoyama, *Sens. Actuators, A* **199**, 43 (2013).
- ¹⁰G. M. Krishna and K. Rajanna, in *Proceedings of the IEEE Tactile Sensor Based on Piezoelectric Resonance: Sensors, 2002*, 12–14 June (2002), Vol. 2, pp. 1643–1647.
- ¹¹M. S. Kim, S. E. Jo, D. H. Kang, H. R. Ahn, and Y. J. Kim, in *The 17th International Conference on a Dome Shaped Piezoelectric Tactile Sensor Array Using Controlled Inflation Technique: Solid-State Sensors, Actuators and Microsystems (TRANSDUCERS & EUROSENSORS*

- XXVII), *2013 Transducers and Eurosensors XXVII*, Barcelona, Spain, 16–20 June (2013), pp. 1891–1894.
- ¹²C. Li, P. M. Wu, S. Lee, A. Gorton, M. J. Schulz, and C. H. Ahn, *J. Microelectromech. Syst.* **17**(2), 334 (2008).
- ¹³S. Petroni, F. Guido, B. Torre, A. Falqui, M. T. Todaro, R. Cingolani, and M. De Vittorio, *Analyst* **137**(22), 5260 (2012).
- ¹⁴S. Petroni, C. La Tegola, G. Caretto, A. Campa, A. Passaseo, M. De Vittorio, and R. Cingolani, in *Proceedings of the 36th International Conference on Micro- and Nano-Engineering (MNE), Aluminum Nitride Piezo-MEMS on Polyimide Flexible Substrates*, Genoa, Italy, 19–22 September (2010), pp. 2372–2375.
- ¹⁵M. Akiyama, Y. Morofuji, T. Kamohara, K. Nishikubo, M. Tsubai, O. Fukuda, and N. Ueno, *J. Appl. Phys.* **100**(11), 114318 (2006).
- ¹⁶M. Akiyama, Y. Morofuji, T. Kamohara, K. Nishikubo, Y. Ooishi, M. Tsubai, O. Fukuda, and N. Ueno, *Adv. Funct. Mater.* **17**(3), 458 (2007).
- ¹⁷C. Giordano, I. Ingrosso, M. T. Todaro, G. Maruccio, S. De Guido, R. Cingolani, A. Passaseo, and M. De Vittorio, *Microelectron. Eng.* **86**, 1204–1207 (2009).
- ¹⁸R. B. Karabalin, M. H. Matheny, X. L. Feng, E. Defaÿ, G. Le Rhun, C. Marcoux, S. Hentz, P. Andreucci, and M. L. Roukes, *Appl. Phys. Lett.* **95**(11), 103111 (2009).
- ¹⁹M. A. Dubois and P. Murali, *J. Appl. Phys.* **89**(11), 6389 (2001).
- ²⁰Z. Wang, Y. Yao, X. Wang, W. Yue, L. Chen, and X. X. Zhang, *Sci. Rep.* **3**, 3127 (2013).
- ²¹T. D. Nguyen, S. Mao, Y. W. Yeh, P. K. Purohit, and M. C. McAlpine, *Adv. Mater.* **25**, 946–974 (2013).
- ²²X. Jiang, W. Huang, and S. Zhang, *Nano Energy* **2**, 1079–1092 (2013).
- ²³V. M. Mastronardi, F. Guido, M. Amato, M. De Vittorio, and S. Petroni, *Microelectron. Eng.* **121**, 59 (2014).
- ²⁴W. C. Young and R. G. Budinas, *Roark's Formulas for Stress and Strain*, 7th ed. (McGraw-Hill, New York, 2002), p. 427.